

Antiproton Evolution in Little Bangs and Big Bang

H. Schade and B. Kämpfer

Forschungszentrum Dresden-Rossendorf,

PF 510119, 01314 Dresden, Germany

TU Dresden, Institut für Theoretische Physik 01062 Dresden, Germany

Abstract

The abundances of antiprotons and protons are considered within momentum-integrated Boltzmann equations describing Little Bangs, i.e., fireballs created in relativistic heavy-ion collisions. Despite of a large antiproton annihilation cross section we find a small drop of the ratio of antiprotons to protons from 170 MeV (chemical freeze-out temperature) until 100 MeV (kinetic freeze-out temperature) for CERN-SPS and BNL-RHIC energies thus corroborating the solution of the previously exposed "antiproton puzzle". In contrast, the Big Bang evolves so slowly that the antibaryons are kept for a long time in equilibrium resulting in an exceedingly small fraction. The adiabatic path of cosmic matter in the phase diagram of strongly interacting matter is mapped out.

I. INTRODUCTION

The abundances of hadrons emerging from relativistic heavy-ion collisions can be described with surprisingly high accuracy by a thermo-statistical model [1]. Over a wide range of bombarding energies essentially two parameters, the temperature T_{chem} and the baryo-chemical potential μ_{chem} , adjusted to experimental data give a smooth curve $T_{chem}(\mu_{chem})$, the so-called chemical freeze-out curve, being an important landmark in the phase diagram of strongly interacting matter. At a given beam energy the variation of T_{chem}, μ_{chem} for various centralities is fairly small [2].

The transverse momentum spectra of various hadron species, at a given beam energy, may also be described by a set of parameters T_{kin}, μ_{kin} , where additionally a flow parameter may be employed. It was argued, e.g. in [3], and later confirmed, e.g. in [4], that $T_{chem} > T_{kin}$ holds in central collisions at high energies. This is often interpreted in a schematic picture as ceasing of inelastic (chemical) reactions at T_{chem} , while in a later stage of the fireball evolution a kinetic freeze-out happens at T_{kin} where the elastic interactions are no longer efficient enough to modify the momentum distributions. A different view was advocated in [5] with $T_{chem} \approx T_{kin}$. In the former scenario there is still "hadronic life" after freezing out the chemical composition, while the latter scenario would mean a sudden termination of inelastic and elastic reactions roughly at the same time.

A possible problem in the commonly accepted first scenario with $T_{chem} > T_{kin}$ was pointed out in [6]: The antiproton (\bar{p}) annihilation cross section is so large that the \bar{p} survival until kinetic freeze-out needs special consideration. This was exposed as the "antiproton puzzle". In [6, 7] it was shown that chemical off-equilibrium combined with multi-hadron reactions give rise to sufficient antiproton regeneration ensuring a moderate drop of the ratio of abundances \bar{p}/p from T_{chem} until T_{kin} for CERN-SPS energies. This fits well in the above first hadro-chemical scenario [8].

It is the aim of this note to reconsider the off-equilibrium evolution of antiprotons in an expanding hadron fireball. We extend the consideration of [7, 8] towards BNL-RHIC and CERN-LHC top energies. In a schematic model we show that the \bar{p}/p ratio at CERN-SPS energies decreases from a given temperature $T_{chem} \approx 170$ MeV until kinetic freeze-out temperature $T_{kin} \approx 100 - 120$ MeV only by a small fraction, while at BLN-RHIC energies the variation of \bar{p}/p in such a temperature interval is even negligible. We expect that at

CERN-LHC energies the latter statement also applies. We employ here a transparent (thus simplified) model to elaborate the features of the evolution towards off-equilibrium after an assumed chemical equilibrium which complies with the mentioned hadro-chemical model [1]. In contrast to this, the involved and sophisticated transport models give a much more complicated description, both for hadro-chemistry in general [9] and for the antiprotons especially [10, 11, 12].

Furthermore, we emphasize similarities and differences to antimatter (baryon) evolution in the early universe after confinement. The adiabatic path of cosmic baryon matter is exhibited in the phase diagram of strongly interacting matter.

The paper is organized as follows. In Section 2 we discuss the appropriate evolution equations for protons (baryons) and antiprotons (antibaryons) coupled by a conservation law. The main emphasis is devoted to applications in relativistic heavy-ion collisions (Section 3) covering situations with baryons and antibaryons being nearly symmetric or very asymmetric. Section 4 describes the cosmic baryon matter. The summary can be found in Section 5. Appendix A sketches the derivation of the used evolution equations.

II. OFF-EQUILIBRIUM EVOLUTION OF ANTIPROTONS

Our starting point is the pair of momentum-integrated Boltzmann equations (see Appendix A)

$$\frac{dY_+}{dx} = -\frac{\Lambda(\xi)}{x^\xi} \left(Y_+(Y_+ - \eta) - Y_{eq}^2 \right), \quad (2.1)$$

$$\frac{dY_-}{dx} = -\frac{\Lambda(\xi)}{x^\xi} \left(Y_-(Y_- + \eta) - Y_{eq}^2 \right), \quad (2.2)$$

where $Y_\pm = n_\pm/s$ are the baryon densities n_\pm normalized to entropy density $s = \frac{2\pi^2}{45} h_{eff} T^3$. We attribute Y_+, n_+ to protons (p) and Y_-, n_- to antiprotons (\bar{p}). h_{eff} is the effective number of degrees of freedom of hadrons in the fireball with comoving volume $V(t)$. Here, we assume a spatially homogeneous fireball and apply for protons and antiprotons the Boltzmann approximation, which is appropriate for the following since $x \equiv m_N/T$ is larger than unity. Therefore, $Y_{eq} = \frac{45}{4\pi^4} \frac{2}{h_{eff}} x^2 K_2(x)$ with the Bessel function K_2 . Both evolution equations refer to pair-wise annihilations and regenerations, thus $Y_+ - Y_- \equiv \eta = const$, i.e. $\dot{Y}_+ = \dot{Y}_-$. The two parameters in the evolution equations, $\Lambda(\xi)$ and η , determine together with initial conditions the off-equilibrium dynamics. In what follows we are going to explore

their interplay for Little Bangs and Big Bang.

For Little Bangs ($\xi = 4$, see Appendix A) one has

$$\Lambda_{(4)} = 3\langle\sigma v\rangle\bar{\tau}m_N^3\frac{2\pi^2}{45}h_{eff}\left(1+\tau\frac{\dot{h}_{eff}}{h_{eff}}\right)^{-1}. \quad (2.3)$$

It encodes essentially the thermally averaged annihilation cross section $\langle\sigma v\rangle$, and \dot{h}_{eff} accounts for the time variation of the effective degrees of freedom. In deriving Eqs. (2.1, 2.2) for Little Bangs we use adiabaticity of the expanding fireball, i.e. $sV = const$. Instead of a specific expansion model we utilize $V/\dot{V} = \bar{\tau}$ with $\bar{\tau}$ as characteristic time scale. This allows us to formulate the evolution as a function of x instead of a function of time.

In the Big Bang ($\xi = 2$, see Appendix A and [13, 14, 15]) the dimensionless factor $\Lambda_{(\xi)}$ reads

$$\Lambda_{(2)} = \langle\sigma v\rangle g_*^{1/2} M_{Pl} m_N \sqrt{\frac{\pi}{45}} \quad (2.4)$$

with $g_*^{1/2} = h_{eff} g_{eff}^{-1/2} \left(1 + \frac{T}{3h_{eff}} \frac{\dot{h}_{eff}}{T}\right)$ and g_{eff} determining the effective degrees of freedom relevant for the energy density, i.e. $e = \frac{\pi^2}{30} g_{eff} T^4$, and M_{Pl} as Planck mass and m_N again as nucleon mass. Clearly, different h_{eff} 's apply in Little Bangs and Big Bang.

Using $\langle\sigma v\rangle = C/m_\pi^2$ with $C = \mathcal{O}(1)$ and with m_π denoting the pion (π^0) mass one arrives for $\bar{\tau} \sim 5$ fm/c at $\Lambda_{(4)} \sim \mathcal{O}(10^4)$ as an estimate (for h_{eff} see below), while $\Lambda_{(2)} \sim \mathcal{O}(10^{21})$ for $g_*^{1/2} \sim 4$ [16] highlights the vast difference of Big Bang and Little Bang dynamics. Actually, the thermally averaged cross section is $\langle\sigma v\rangle = \frac{\int_{2x}^{\infty} d\xi \xi^2 (\xi^2 - 4x^2) K_1(\xi) \sigma(p_{lab})}{4x^4 K_2^2(x)}$ [13] with $p_{lab} = T\xi\sqrt{\xi^2 - 4x^2}/(2x)$, see also [17]. Employing $\sigma(p_{lab}) = (40p_{lab,GeV/c}^{-0.5} + 24p_{lab,GeV/c}^{-1.1})$ mb [7] or $(38 + 35p_{lab,GeV/c}^{-1})$ mb for the $\bar{p}p$ annihilation cross section one arrives at $\langle\sigma v\rangle \simeq 42.5 - 47$ mb in the temperature interval 170 - 100 MeV or 51.5 mb fairly independent of T , thus yielding $C \sim 2$.

III. RESULTS FOR LITTLE BANGS

Equations (2.1, 2.2) are of Riccati type with no general analytical solution in closed form. The solutions, to be found numerically, depend on $\Lambda_{(\xi)}$ and the initial conditions (encoded in η). For the latter ones we employ $T_{chem} = T_0 = 170$ MeV and $\mu_{chem} = \mu_0 = 250$ MeV (SPS top energy resulting in $n_-/n_+ = 0.052$) or $\mu_{chem} = \mu_0 = 25$ MeV (RHIC top energy resulting in $n_-/n_+ = 0.75$), thus neglecting a possi-

ble small change of chemical freeze-out temperature when going from SPS to RHIC but catching the typical values extracted in the data analysis [1, 2]. SPS energies are in the realm $\mu_{chem} > T_{chem}$, while RHIC and LHC operate in the region $\mu_{chem} < T_{chem}$. A good approximation of h_{eff} is provided by $h_{eff}(T) = h_1 + \hat{b}(T - T_1) + \hat{c}(T - T_1)^2$ with $\hat{b} = [h_2 - h_1 - (h_3 - h_1)(T_2 - T_1)^2/(T_3 - T_1)^2] / [T_2 - T_1 - (T_2 - T_1)^2/(T_3 - T_1)]$ and $\hat{c} = (h_3 - h_1)/(T_3 - T_1)^2 - \hat{b}/(T_3 - T_1)$ and $(T_1, T_2, T_3, h_1, h_2, h_3) = (0.100, 0.150, 0.175, 3.0, 9.8, 17.5)$ for small chemical potentials as appropriate for RHIC top energies and $(0.100, 0.150, 0.175, 5.411, 13.150, 21.750)$ for an isentrope with entropy per baryon equal to 23 as appropriate for SPS top energy. These values are for the resonance gas model with the first hundred hadronic states as used in [1] and for temperatures in GeV. While the scales $\langle\sigma v\rangle$ and $\bar{\tau}$ as well as h_{eff} are condensed into one dimensionless parameter $\Lambda_{(4)}$ which would be useful for $h_{eff} = const$, the strong variation of h_{eff} in the considered temperature range along isentropic trajectories makes $\Lambda_{(4)}$ not a concise characteristic quantity. Therefore, we present the results for various values of C to expose the influence of annihilations and to discriminate them from diminishing densities due to expansion.

In Fig. 1 the change of n_-/n_+ (denoted by \bar{p}/p) as a function of the temperature is exhibited. We note that, similar to the consideration in [7], the ratio drops only by a small fraction even when extending the evolution down to a temperature of 100 MeV. The reason is the small change of Y_{\pm} . The experimental mid-rapidity value of \bar{p}/p is 0.058 ± 0.005 (statistical error) in central collisions of Pb + Pb at $E_{beam} = 158$ AGeV [18]. Clearly, our above mentioned initial value is already somewhat below this experimental value. If one would change μ_0 to 235 MeV, being still in the range of admissible values according to [1], the start value would be $n_-/n_+ = 0.063$ and all curves exhibited in Fig. 1 are then upshifted, roughly by factor 1.2. As a consequence, values of $C < 4$ would be compatible with the data. While this range of C is realistic, such a fine tuning is not appropriate given the schematic character of our model (use of a characteristic time scale $\bar{\tau}$ for the expanding fireball, no feeding etc.). This refrains us from considering further details like the centrality dependence. Nevertheless, one may consider the beam energy systematics for central collisions. Instead of individually selected values of μ_{chem} and T_{chem} , one may use a global fit of many hadron ratios with the parametrization [1], $\mu_{chem} = 1303 \text{ MeV} / (1 + 0.286\sqrt{s_{NN}}/\text{GeV})$ and $T_{chem} = 162 \text{ MeV} \left(1 - (0.7 + \exp[(\sqrt{s_{NN}}/\text{GeV} - 2.9)/1.5])^{-1}\right)$ (where $\sqrt{s_{NN}}$ is in GeV) and get initial values for n_-/n_+ being 15%, 1.5%, 18%, 30% and 29% larger than the ex-

perimental ratios \bar{p}/p quoted in [18] for central Pb + Pb collisions at SPS beam energies of 158, 80, 40, 30 and 20 AGeV. The offset of n_-/n_+ above the experimental \bar{p}/p value [19] at $\sqrt{s_{NN}} = 200$ GeV is 36% according to this parametrization. With the exception of the data situation for beam energy of 80 AGeV, there is room for a 20% drop, in average, of \bar{p}/p towards kinetic freeze-out, consistent with the results in Fig. 1.

In contrast to the ratio \bar{p}/p , the densities rapidly change with dropping temperature, as exhibited in Fig. 2. A notable point is the increasingly strong departure of n_- from the chemical equilibrium value n_-^{eq} towards kinetic freeze-out. For this comparison we have determined n_{\pm}^{eq} by $sY_{eq} \exp(\pm\mu/T)$ with μ from the resonance gas model along the isentropic curve imposing baryon conservation (a convenient parametrization is provided by $\mu = \tilde{a}/T^{\tilde{x}} + \tilde{b}$ with $(\tilde{x}, \tilde{a}, \tilde{b}) = (1, 0.045198563, -0.015873836) - T$ and μ in units of GeV). The emerging relation $n_+^{eq} > n_+$ (see Fig. 2) is surprising at the first glance. In fact, baryon conservation enforces $n_N > n_N^{(0)}V(t=0)/V(t>0)$ for the net nucleon density. Since the antibaryon density in the situation at hand is significantly smaller than the baryon density, the nucleon density also decreases slower than $V(t=0)/V(t>0)$. As our evolution equations impose pair-wise annihilations and regenerations, for $n_+ \gg n_-$, n_+ goes approximately with $V(t=0)/V(t)$, while the fiducial density obeys $n_+^{eq} > n_+^{(0)}V(t=0)/V(t>0)$. This ostensible ambiguity can be resolved by introducing effective chemical potentials in line with [6, 7, 8]. This, however, is not necessary for the present purposes, as the combination $n_+^{eq}n_-^{eq}$ (or $Y_+^{eq}Y_-^{eq}$) enter the evolution equations, and neither n_+^{eq} nor n_-^{eq} separately: In the employed Boltzmann approximation, the chemical potentials cancel in $Y_+^{eq}Y_-^{eq} = Y_{eq}^2$. Discarding this gain (or recombination) term would result in a significantly reduced ratio \bar{p}/p , thus emphasizing the importance of the back-reaction, as already stressed in [6, 7, 8]. (In [7] the regeneration term is of utmost importance to counteract the stronger annihilations at the total baryon content.)

Summarizing, the inspection of Fig. 2 reveals the strong deviation from equilibrium, i.e., despite of the large annihilation cross section the expansion is too rapid to maintain chemical equilibrium of antiprotons. For larger values of $\langle\sigma v\rangle$ parameterized by C , n_- follows more closely the fiducial density n_-^{eq} and, as a consequence, the antiproton to proton ratio drops stronger during cooling (see also Fig. 1). A larger value of the expansion time scale $\bar{\tau}$ reduces also the ratio \bar{p}/p : For $\bar{\tau} = 10$ fm/c we get 0.040 at $T = 100$ MeV. In contrast, a shorter expansion time scale keeps the ratio at higher values, say 0.048 for $\bar{\tau} = 3$ fm/c. As n_+ is

essentially not modified, one can infer the corresponding values of n_- from these numbers.

Reference [1] (first quotation) states that the thermo-statistical model applies not only to selected ratios of hadron yields but also to yields themselves. It is instructive, therefore, to consider the evolution of the yields from chemical freeze-out towards kinetic freeze-out temperatures. We normalize the yields according to $(n_i V)_{100 \text{ MeV}} / (n_i V)_{170 \text{ MeV}}$ and exhibit in Fig. 3 the dependence on $C = \langle \sigma v \rangle / m_\pi^2$. The yield of antiprotons depends smoothly on C ; values $C > 3$ would cause a sizeable annihilation which would obscure the hadro-chemistry picture.

For RHIC energy the same features hold. However, different initial conditions cause some different evolution: The ratio \bar{p}/p is fairly insensitive to C , see Fig. 4. The departure from equilibrium for protons is nearly as strong as for antiprotons, as shown in Fig. 5. (Here, the above parametrization of $\mu(T)$ with $(\tilde{x}, \tilde{a}, \tilde{b}) = (4.8, 2.2671929 \times 10^{-6}, 0.013797031)$ applies.) Also the yields in Fig. 6 drop with increasing values of C as they are more dragged by the respective equilibrium values. For $C < 10$ the reduction via annihilation is less than 10% thus not invalidating the consistency of hadro-chemistry with a late kinetic freeze-out. Experimentally, one finds $\bar{p}/p = 0.731 \pm 0.011 \pm 0.062$ [19] in central collisions Au + Au at $\sqrt{s_{NN}} = 200$ GeV which is fairly independent of centrality. This value compares well with the results in Fig. 4, even for large C .

For smaller values of μ_{chem} the difference of n_- and n_+ becomes smaller: Annihilation diminishes both n_- and n_+ by the same amount thus keeping the ratio n_-/n_+ nearly constant. This consideration applies in particular for LHC. In contrast, for the above baryon-antibaryon asymmetric situation at SPS, given by a larger value of μ_{chem} , the annihilation of p by the small admixture of \bar{p} is not severe, and only the evolution equation for n_- is sufficient, as exploited in [7].

Resolving the "antiproton puzzle" means demonstrating that the \bar{p}/p ratio does not change noticeably from T_{chem} until T_{kin} . At high beam energies (say, for RHIC and LHC energies) corresponding to smaller values of the normalized particle-antiparticle number difference η this seems to be fairly robust. At SPS one sees already a sensitivity to the interplay of thermally averaged annihilation cross section and expansion dynamics. At AGS and later on planned FAIR energies one expects a stronger drop of the \bar{p}/p ratio. However, the differences of T_{chem} and T_{kin} may be much smaller so that again annihilation is less severe.

Our results base on a few assumptions which we recollect here: (i) kinetic equilibrium (which is left at the kinetic freeze-out, see [20] for dealing with the freeze-out itself); (ii) spatial homogeneity; (iii) expansion dynamics characterized by one time scale; (iv) restriction to one hadron species, p, \bar{p} (the other hadrons are implicitly in the heat bath, encoded in h_{eff} [35]); (v) chemical equilibrium at T_{chem}, μ_{chem} ; (vi) detailed balance and unitarity. Items (i - v) are relaxed in transport codes, which also attempt to include (vi). We insist here to arrive at a qualitative and transparent understanding of an aspect of chemical freeze-out. Items (i) and (ii) are related with the derivation of the employed form of the momentum integrated Boltzmann equation, see [13] for details. Item (iii) refers to the fact that we consider a specific expansion pattern of the fireball (which is assumed to contain a homogeneous matter distribution according to item (ii)) characterized by $V/\dot{V} = \bar{\tau}$ with $\bar{\tau}$ as expansion time scale, see Appendix A. Item (v) fixes the initial conditions in agreement with the thermo-statistical model [1].

Strictly speaking, item (vi) refers to the balance $p + \bar{p} \leftrightarrow X + \bar{X}$ as the underlying Boltzmann equation including a binary collision kernel leads to our evolution equations (2.1, 2.2). One may think, however, that both X and \bar{X} represent clusters of pions. Such states X, \bar{X} are successfully considered in [21] as two-meson doorway states coupling in turn to multi-pion states. This approach, also known as minimal two-body model, realizes the nearest threshold dominance and describes the $p\bar{p}$ annihilation data in the energy region relevant for our purposes. It bridges to [6, 7], where such multi-pion collisions were considered as key to resolve the antiproton puzzle together with chemical off-equilibrium in the pion component. As further possible ingredients one may consider the role of baryon excitations (as sources for further annihilations and regenerations) and feeding of the ground state baryons eventually observed, as done in [22] for RHIC energy.

IV. ANTIBARYONS IN BIG BANG

Due to the numerically large value of $\Lambda_{(2)}$, the evolution of n_{\pm} follows closely the equilibrium values n_{\pm}^{eq} for a long time. In other words, Y_{\pm} are dragged by Y_{\pm}^{eq} as evidenced by solving numerically Eqs. (2.1, 2.2). In the temperature region $T > 1$ MeV, $Y_{\pm} \approx Y_{\pm}^{eq}$ represent highly accurate solutions of the evolution equations. Freeze-out of the antinucleon annihilation happens at temperatures being considerably lower than the MeV scale [15] thus

yielding an exceedingly small antibaryon density in the assumed homogeneous scenario (for inhomogeneous scenarios cf. [23]). Indeed, using $n_{\pm} \approx n_{\pm}^{eq} = sY_{eq} \exp\{\pm\mu/T\}$, one finds a rapid dropping of the scaled antibaryon density, represented by n_-/T^3 , with decreasing temperature, see top panel of Fig. 7 (μ is determined by Eq. (4.1) below). For the given small surplus of baryons, the scaled density n_+/T^3 follows closely n_-/T^3 until 40 MeV; on the exhibited scale in Fig. 7 the difference of n_+/T^3 to n_-/T^3 is not visible. Below that temperature of 40 MeV, however, n_+/T^3 stays approximately constant at $\eta s/T^3$; the still continuing annihilations diminish n_+/T^3 only marginally [36] since n_-/T^3 became small. The turn of n_+/T^3 from dropping to the approximately constant value near $\eta s/T^3$ at temperatures of 40 MeV is entirely determined by the value of η [24] which quantifies the baryon surplus, encoding also the chemical potential.

In the cosmic evolution, say after confinement, $\eta \sim 10^{-10}$ is presumably realized, governed by the observed ratio of baryons to photons being 6.12×10^{-10} (Λ CDM 3-year WMAP-only data [25]) and relying on adiabaticity. This ratio also determines the adiabatic path of cosmic matter after confinement until the onset of primordial nucleosynthesis at $T \lesssim 1$ MeV, see Fig. 8 which is based on baryon conservation expressed by

$$\mu = T \operatorname{arsh} \left(\eta \frac{2\pi^4}{45} \frac{h_{eff}}{2} \frac{1}{x^2 K_2(x)} \right). \quad (4.1)$$

Strictly speaking, this equation applies for $h_{eff} = \text{const}$ and for situations where nucleons are essentially the carriers of baryon charge. Accordingly, the cosmic baryo-chemical potential μ evolves from 10^{-6} MeV at $T = 170$ MeV towards $m_N \sim 938$ MeV prior to nucleosynthesis at $T < 1$ MeV [24, 26]. Features of Eq. (4.1) are: (i) $\min(\mu) = \mathcal{O}(m_N \eta)$, (ii) $\max(\mu) = m_N$, (iii) crossing the $\mu = T$ line at $T \approx m_N / (-\log \eta + \dots)$ (this is the point where the difference of n_+ and n_- becomes large with dropping temperature: n_+/T^3 then stays approximately constant at $\eta(2\pi^2/45)h_{eff}$, while n_-/T^3 continues dropping exponentially, see Fig. 7 and [24]), (iv) before the region $\mu \sim T$ is reached, the temperature drops as $T \propto m_N / (\log(\mu/m_N \eta) + \dots)$. The \dots in items (iii) and (iv) are for subleading terms. The variation of h_{eff} with temperature, according to the resonance gas model, pulls down the isentropic curve (solid line) for $\mu < 1$ keV so that the crossing with the dashed line occurs at a temperature of 165 MeV (instead of 225 MeV). For $\mu > 1$ keV, the results of the resonance gas model with adiabaticity and baryon conservation are on top of the solid line.

For an orientation, in Fig. 8 also chemical freeze-out points in relativistic heavy-ion colli-

sions from the analysis in [1] (first quotation) are exhibited. At the freeze-out temperature of about 160 MeV in Little Bangs at RHIC the baryo-chemical potential is about 10^7 times larger than in Big Bang. Otherwise, when the baryo-chemical potential values of Little Bangs at RHIC is achieved, the temperature in Big Bang is about 40 MeV (see also [27]), being surprisingly high.

During the evolution of matter after electro-weak symmetry breaking at $T \sim \mathcal{O}(100 \text{ GeV})$ down to confinement at $T_c \sim \mathcal{O}(200 \text{ MeV})$, the strongly interacting matter dominates by far the pressure, the energy density and the entropy density [28]. The masses of carriers of baryon charge change in the confinement transition. Below 160 MeV the energy density is dominated by electro-weak matter for a long time including primordial nucleo-synthesis, see bottom panel of Fig. 7. Pions are exceptional, as they are sizeable in number and energy density contribution down to 5 MeV. The bottom panel of Fig. 7 evidences also the slow relative increase of the scaled baryonic energy density; much later (before "recombination") it will exceed the electro-weak matter thus turning the radiation universe into a matter dominated universe.

V. SUMMARY

In summary we contrast the baryonic antimatter evolution in Little Bangs (i.e. bulk matter of fireballs created in relativistic heavy-ion collisions) and Big Bang from confinement towards the onset of primordial nucleo-synthesis. To expose the similarities and differences we focus on antiprotons in heavy-ion collisions and nucleons in the cosmic evolution within a schematic kinetic description neglecting the explicit coupling to other hadron states. The vast differences of Little Bangs and Big Bang are impressively described by the huge difference of the dimensionless parameters $\Lambda_{(\xi)}$ governing the chemical freeze-out dynamics. In addition, the scaled net baryon densities encoded in η are also drastically different.

In Little Bangs, the ratio \bar{p}/p drops only by a tiny amount from the established chemical freeze-out temperature (which is defined by a multitude of other hadron abundances) until kinetic freeze-out for RHIC conditions, where antiprotons appear in a sizeable fraction. For a larger asymmetry of antiprotons to protons (as realized for SPS conditions) the ratio \bar{p}/p changes still by a sufficiently small amount to maintain the consistency of the thermo-statistical model for hadron chemistry. The thermo-statistical model is an important tool

for mapping out the phase diagram of strongly interacting matter in the $T - \mu$ plane. In so far, it is important that its features conform with a detailed description of heavy-ion collisions.

In homogeneous scenarios for the Big Bang, the chemical equilibrium is maintained for a long time thus resulting in an exceedingly small fraction of primordial antibaryons [15]. An interesting point is the adiabatic path of cosmic baryons through the phase diagram of strongly interacting matter and the related temperature of about 40 MeV (determined by η) during the orders-of-magnitude change of the chemical potential turning cosmic baryon matter from $\mu/T \ll 1$ into $\mu/T \gg 1$.

Acknowledgments

The work is supported by BMBF 06DR136, GSI and EU-I3HP. The authors gratefully acknowledge stimulating discussions with E. Grosse.

APPENDIX A: MOMENTUM-INTEGRATED BOLTZMANN EQUATION

Let be $L_i N_i = C_i$ the Boltzmann transport equation for particles of species i , where L_i is the covariant Liouville operator, $L_i = p_i^\mu \frac{\partial}{\partial x^\mu} - \Gamma_{\alpha\beta}^\mu p_i^\alpha p_i^\beta \frac{\partial}{\partial p_i^\mu}$ with affine connection $\Gamma_{\alpha\beta}^\mu$ and Greek indices running from 0 - 3 (Einstein's sum convention applies only for them). C_i may be a general source term modifying the free-stream of the distribution function $N_i(x, p)$ by collisions and feeding by decays. A consequence of the structure of the Liouville operator is $N_{i;\alpha}^\alpha = \int L_i N_i \Pi_i$ [29, 30] and thus with the Boltzmann equation one gets $N_{i;\alpha}^\alpha = \int C_i \Pi_i$, where the coordinate-independent momentum element for particle of species i is in the notation of [30] $\Pi_i = d_i (2\pi)^{-3} \sqrt{-g} \frac{d^3 p_i}{|p_i^0|}$ with the fundamental determinant $-g$, to be built of the metric tensor $g_{\mu\nu}$, and particle degeneracy d_i ; the semicolon stands for the coordinate-covariant derivative. The particle momenta p_i^μ are normalized to rest masses m_i as $g_{\mu\nu} p_i^\mu p_i^\nu = -m_i^2$. The particle current is defined by $N_i^\alpha \equiv \int N_i p_i^\alpha \Pi_i$. For an observer moving with four-velocity v_α the corresponding particle density is $n_i = -v_\alpha N_i^\alpha$.

We consider here bulk matter in sufficiently small volume elements where matter looks isotropically and homogeneously. Moreover, the matter is provided to be in collisional (i.e., thermal) equilibrium so that a common flow field $u^\alpha(x)$ can be attributed to all particle

species. This means, $N_i^\alpha = n_i u^\alpha$ [31]. Synchronizing the observer velocity with the flow by introducing a comoving coordinate system where $u^\alpha = g_0^\alpha \equiv \delta_0^\alpha$, the l.h.s. of the balance equation for the density n_i , $(n_i u^\alpha)_{;\alpha} = \int C_i \Pi_i$, becomes $\frac{1}{\sqrt{-g}}(\sqrt{-g} n_i g_0^\alpha)_{;\alpha} = \frac{1}{\sqrt{-g}}(\sqrt{-g} \dot{n}_i)$, where the dot means time derivative in the respective comoving coordinate system. Introducing with the reasoning of [30] a comoving three-volume V , defined, e.g., by $(n_{con} V) = 0$ for a conserved charge density n_{con} or by entropy conservation, $(sV) = 0$, the l.h.s. of the considered balance equation may be written as $\frac{1}{V}(\dot{n}_i V)$.

Binary elastic collisions, $i + i' \leftrightarrow i'' + i'''$, cancel out the r.h.s. of the balance equation as they represent collisional invariants. For the moment being, we focus on binary annihilation processes, $i + \bar{i} \leftrightarrow X + \bar{X}$ [32]. In the absence of Bose condensation or Fermi degeneracy effects and with the assumption that species X and \bar{X} have equilibrium distributions, the collision term $\int C_i \Pi_i$ can be evaluated (see [13, 32] for details) to result in the master type equation

$$\dot{n}_i + n_i \frac{\dot{V}}{V} = -\langle \sigma v \rangle (n_i n_{\bar{i}} - n_i^{eq} n_{\bar{i}}^{eq}) \quad (\text{A1})$$

and an analog equation for \bar{i} by the replacement $i \rightarrow \bar{i}$. For Robertson-Walker-Friedmann cosmology, where strict isotropy and homogeneity is applied, this is an often derived and applied equation, see [13, 14, 15, 32], and is referred to as momentum-integrated Boltzmann equation. In heavy-ion collisions such an equation, supplemented by decay terms, is used too, for instance in [22]. In order to apply the above arguments, however, special flow symmetries must be required. We consider examples below. (Other approaches [33] to rate equations use a spatial average over the expanding fireball, where a Lorentz factor for transforming the time coordinate to the external coordinate system occurs additionally.)

We follow further the arguments in [13, 32] and reformulate the rate equation (A1), instead as time evolution equation with respect to comoving or proper observer time, as evolution equation with respect to temperature T : Define the yields $Y_i = n_i/s$, use the definition of the comoving volume V by $(sV) = 0$, and introduce the new variable $x = m_N/T$ to arrive at

$$\frac{dY_i}{dx} = -\langle \sigma v \rangle (Y_i Y_{\bar{i}} - Y_i^{eq} Y_{\bar{i}}^{eq}) \frac{m_N^3}{x^4} \frac{3V}{\dot{V}} \frac{2\pi^2}{45} h_{eff} \left(1 + \frac{\dot{h}_{eff}}{h_{eff}} \frac{T}{3\dot{T}} \right). \quad (\text{A2})$$

Clearly, further evolution equations are still needed describing the expansion dynamics of the system under consideration. For our schematic discussion in heavy-ion collisions we put $V/\dot{V} = \bar{\tau}$ with $\bar{\tau}$ as characteristic expansion time. If the flow pattern is assumed to be

specific, the relevant time scales are henceforth prescribed. Examples for simple flow patterns are the four-velocities (i) $\bar{u}^\mu = (\text{ch}\hat{\eta}, 0, 0, \text{sh}\hat{\eta})$, (ii) $\bar{u}^\mu = (\text{ch}\hat{\eta}, \text{sh}\hat{\eta} \cos \phi, \text{sh}\hat{\eta} \sin \phi, 0)$, (iii) $\bar{u}^\mu = (\text{ch}\hat{\eta}, \text{sh}\hat{\eta} \sin \theta \cos \phi, \text{sh}\hat{\eta} \sin \theta \sin \phi, \text{sh}\hat{\eta} \cos \theta)$ with $\hat{\eta} = \frac{1}{2} \log((\bar{t} + \zeta)/(\bar{t} - \zeta))$, for (i) $\zeta = \bar{z}$, (ii) $\zeta = \sqrt{\bar{x}^2 + \bar{y}^2}$ and (iii) $\zeta = \sqrt{\bar{x}^2 + \bar{y}^2 + \bar{z}^2}$ describing (i) purely longitudinal (Bjorken), (ii) axial-symmetric transverse und (iii) spherical expansion yielding with $\tau = \sqrt{\bar{t}^2 - \zeta^2}$ for $(1/V)(dV/d\tau)$ (i) $1/\tau$, (ii) $2/\tau$, and (iii) $3/\tau$ (here, $\bar{t}, \bar{x}, \bar{y}, \bar{z}$ are Cartesian coordinates in Minkowski space-time where \bar{u}^α refers to; θ and ϕ are usual cylinder or polar coordinates). The approximation leading to Eqs. (2.1, 2.2) consists in the replacement of the latter ratios by the inverse of a characteristic time scale, $1/\bar{\tau}$. Executing the transformation to the comoving coordinates via $u^\alpha = \frac{\partial x^\alpha(\bar{x})}{\partial \bar{x}^\mu} \bar{u}^\mu$ yields $u^\alpha = g_0^\alpha$; the line elements in the comoving coordinates read (i) $ds^2 = -d\tau^2 + dx^2 + dy^2 + \tau^2 d\hat{\eta}^2$, (ii) $ds^2 = -d\tau^2 + \tau^2 d\hat{\eta}^2 + \tau^2 \text{sh}^2 \hat{\eta} d\phi^2 + dz^2$, (iii) $ds^2 = -d\tau^2 + \tau^2 d\hat{\eta}^2 + \tau^2 \text{sh}^2 \hat{\eta} d\theta^2 + \tau^2 \text{sh}^2 \hat{\eta} \sin^2 \theta d\phi^2$ representing time-orthogonal (Gaussian) coordinates, as required to arrive at Eq. (A1).

In Robertson-Walker-Friedmann cosmology with the line element $ds^2 = -dt^2 + R^2(t)d\vec{x}^2$ the comoving velocity is as mentioned above; $R(t)$ is the scale factor. The Einstein equations govern the dynamics. For conformal flat three-space and without cosmological constant one has [34] $\dot{V}/V = 3\dot{R}/R = 3\sqrt{\frac{8\pi}{3}}G_N e$ with Newton's constant $G_N = M_{Pl}^{-2}$ and the energy density $e = \frac{\pi^2}{30}g_{eff}T^4$. Combining these quantities appropriately one gets Eqs. (2.1, 2.2) with (2.4) from (A2) as compact notation of the evolution equations for protons or nucleons ($i \rightarrow +$) and antiprotons or antinucleons ($\bar{i} \rightarrow -$).

-
- [1] A. Andronic, P. Braun-Munzinger, J. Stachel, Nucl. Phys. A 772 (2006) 167;
F. Becattini, J. Manninen, M. Gazdzicki, Phys. Rev. C 73 (2006) 044905;
J. Cleymans, H. Oeschler, K. Redlich, S. Wheaton, Phys. Rev. C 73 (2006) 034905.
- [2] J. Cleymans, B. Kämpfer, M. Kaneta, S. Wheaton, N. Xu, Phys. Rev. C 71 (2005) 054901;
J. Cleymans, B. Kämpfer, S. Wheaton, Phys. Rev. C 65 (2002) 027901.
- [3] B. Kämpfer, hep-ph/9612336.
- [4] B.I. Abelev et al. (STAR), Phys. Rev. Lett. 97 (2006) 152301;
J. Adams et al. (STAR), Phys. Rev. Lett. 92 (2004) 112301, Phys. Rev. C 71 (2005) 064902;
H. Appelshäuser et al. (NA49), Eur. Phys. J. C 2 (1998) 661.

- [5] W. Broniowski, W. Florkowski, Phys. Rev. C 65 (2002) 064905; Phys. Rev. Lett. 87 (2001) 272302.
- [6] R. Rapp, E.V. Shuryak, Phys. Rev. Lett. 86 (2001) 2980.
- [7] R. Rapp, nucl-th/0202059.
- [8] R. Rapp, Phys. Rev. C 66 (2002) 017901.
- [9] S.A. Bass et al., Phys. Rev. Lett. 81 (1998) 4092;
L.V. Bravina et al., Phys. Rev. C 60 (1999) 024904.
- [10] W. Cassing, Nucl. Phys. A 700 (2002) 618.
- [11] Y. Pang, D.E. Kahana, S.H. Kahana, H. Crawford, Phys. Rev. Lett. 78 (1997) 3418.
- [12] M. Bleicher, M. Belkacem, S.A. Bass, S. Soff, H. Stöcker, Phys. Lett. B 485 (2000) 133.
- [13] P. Gondolo, G. Gelmini, Nucl. Phys. B 360 (1991) 145.
- [14] K. Griest, D. Seckel, Nucl. Phys. B 283 (1987) 681.
- [15] R.J. Scherrer, M.S. Turner, Phys. Rev. D 34 (1986) 1585, 3263.
- [16] M. Hindmarsh, O.Philipsen, PoS JHW2005 (2005) 007.
- [17] J. Kapusta, A. Mekjan, Phys. Rev. D 33 (1986) 1304.
- [18] C. Alt et al. (NA49), Phys. Rev. C 73 (2006) 044910.
- [19] S.S. Adler et al. (PHENIX), Phys. Rev. C 69 (2004) 034909;
J. Adams et al. (STAR), Phys. Rev. Lett. 92 (2004) 112301.
- [20] V.K. Magas, L.P. Csernai, E. Molnar, Eur. Phys. J. A 31 (2007) 854.
- [21] J. Vandermeulen, Z. Phys. C 37 (1988) 563;
S. Mundigl, M.J. Vicente Vacas, W. Weise, Nucl. Phys. A 523 (1991) 499, Z. Phys. A 338 (1991) 103.
- [22] P. Huovinen, J.I. Kapusta, Phys. Rev. C 69 (2004) 014902.
- [23] J.B. Rehm, K. Jedamzik, Phys. Rev. D 63 (2001) 043509;
S. Matsuura, S. Fujimoto, S. Nishimura, M. Hashimoto, K. Sato, Phys. Rev. D 72 (2005) 123505.
- [24] B. Kämpfer, M. Bluhm, J. Phys. G 31 (2005) S1141.
- [25] D.N. Spergel et al., Astrophys. J. Suppl. 170 (2007) 377.
- [26] M.J. Fromerth, J. Rafelski, astro-ph/0211346.
- [27] P. Braun-Munzinger, J. Wambach, Phys. J. 5 (2006) 41.
- [28] M. Hindmarsh, O. Philipsen, Phys. Rev. D 71 (2005) 087302.

- [29] J.M. Stewart, Non-equilibrium relativistic kinetic theory, Lecture Notes in Physics 10, Springer-Verlag Berlin - Heidelberg 1971.
- [30] R.V. Wagoner, The early universe, in Les Houches 1979, Physical cosmology, (Eds.) R. Balian, J. Audouze, D.N. Schramm, p. 398.
- [31] W. Zimdahl, Phys. Rev. D 57 (1998) 2245.
- [32] E.W. Kolb, M.S. Turner, The early universe, Addison-Wesley Publishing Company 1990, Sections 5.2 and 6.4.
- [33] T. Biro, H.W. Barz, B. Lukacs, J. Zimanyi, Phys. Rev. C 27 (1983) 2695;
B. Kämpfer, O.P. Pavlenko, Z. Phys. C 62 (1994) 491.
- [34] J. Bernstein, Kinetic theory in the expanding universe, Cambridge University Press 1988.
- [35] A more detailed picture is considered in [22], where coupled rate equations for many hadron species are solved in the dynamical background of 2 + 1 dimensional hydrodynamics.
- [36] Given $\Lambda_{(2)} \sim \mathcal{O}(10^{21})$, only for hypothetical values of $\eta < 10^{-16}$ the antinucleon contribution could be sizeable due to chemical freeze-out at $T \lesssim 30$ MeV, as can be found in solving numerically Eqs. (2.1, 2.2).

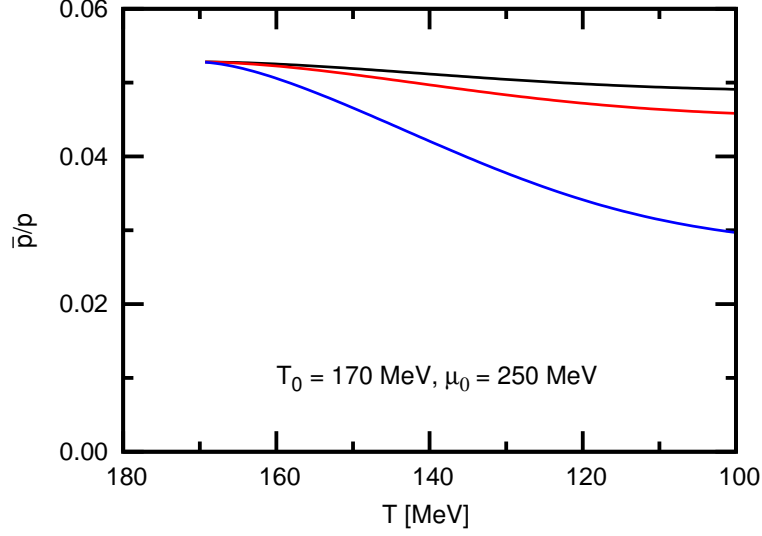


FIG. 1: (Color online) The ratio of antiprotons to protons as a function of temperature for various values of $C = 1, 2, 10$ (from top to bottom). Initial conditions for SPS as described in the text.

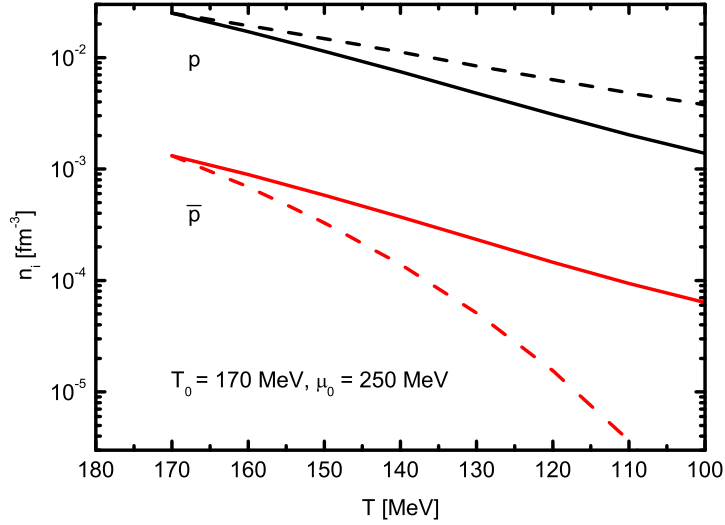


FIG. 2: (Color online) The proton density and antiproton density as a function of temperature. Initial conditions for SPS. Solid curves: actual densities n_{\pm} for the off-equilibrium evolution (i.e. solutions of Eqs. (2.1, 2.2)), dashed curves: fiducial equilibrium densities n_{\pm}^{eq} which need special explanation (see text). For $C = 2$.

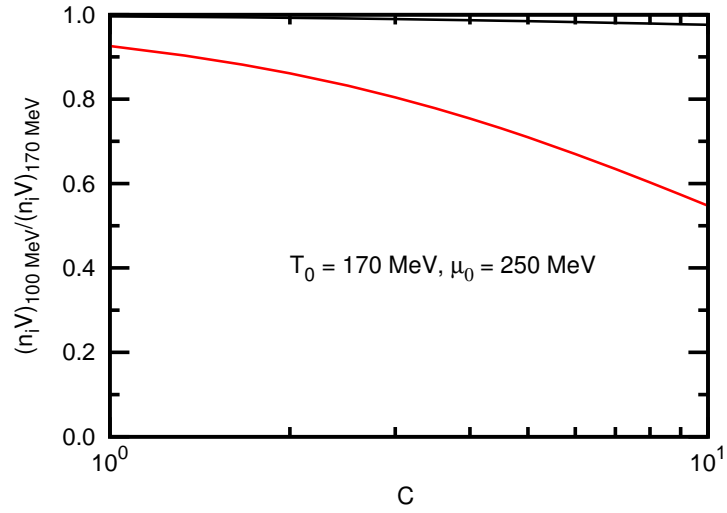


FIG. 3: (Color online) The proton yield (upper curve) and antiproton yield (lower curve) at 100 MeV normalized to those at 170 MeV as a function of C . Initial conditions for SPS.

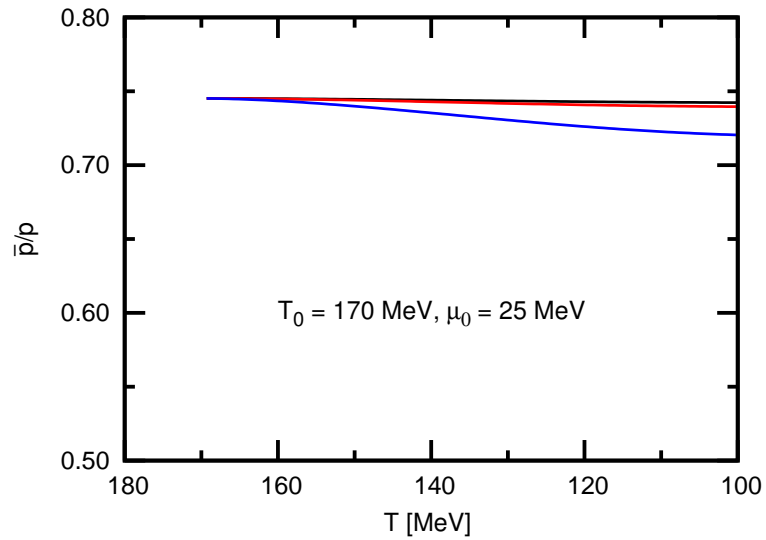


FIG. 4: (Color online) As Fig. 1 but for RHIC initial conditions.

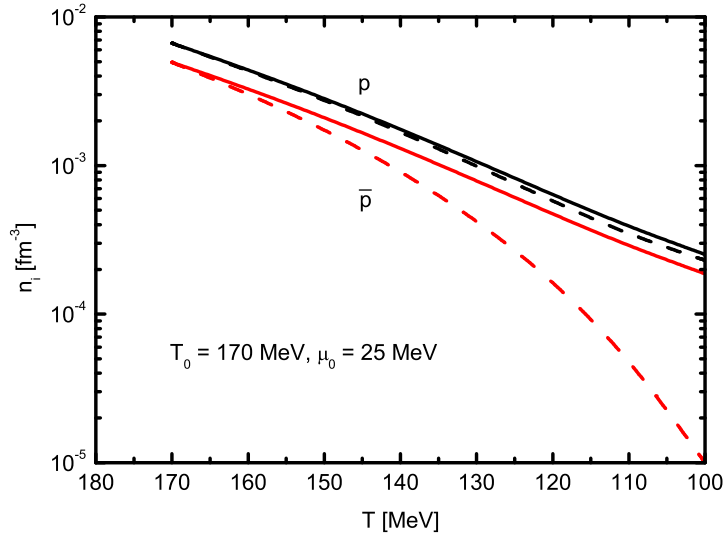


FIG. 5: (Color online) As Fig. 2 but for RHIC initial conditions.

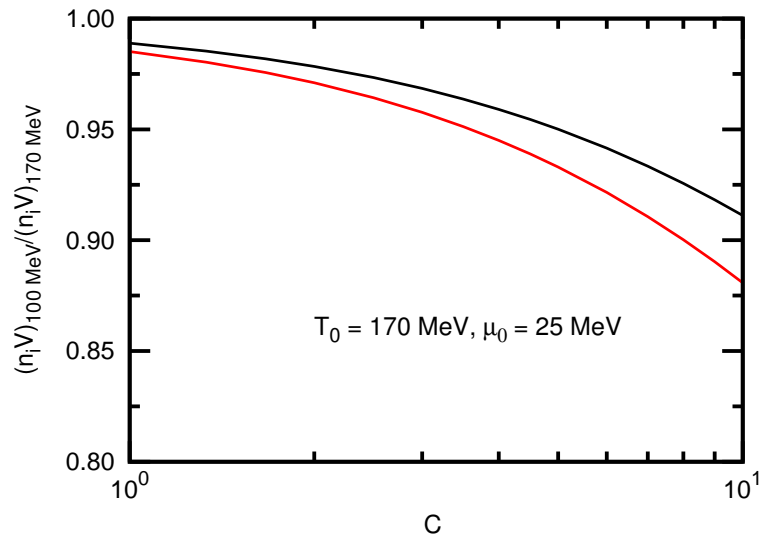


FIG. 6: (Color online) As Fig. 3 but for RHIC initial conditions.

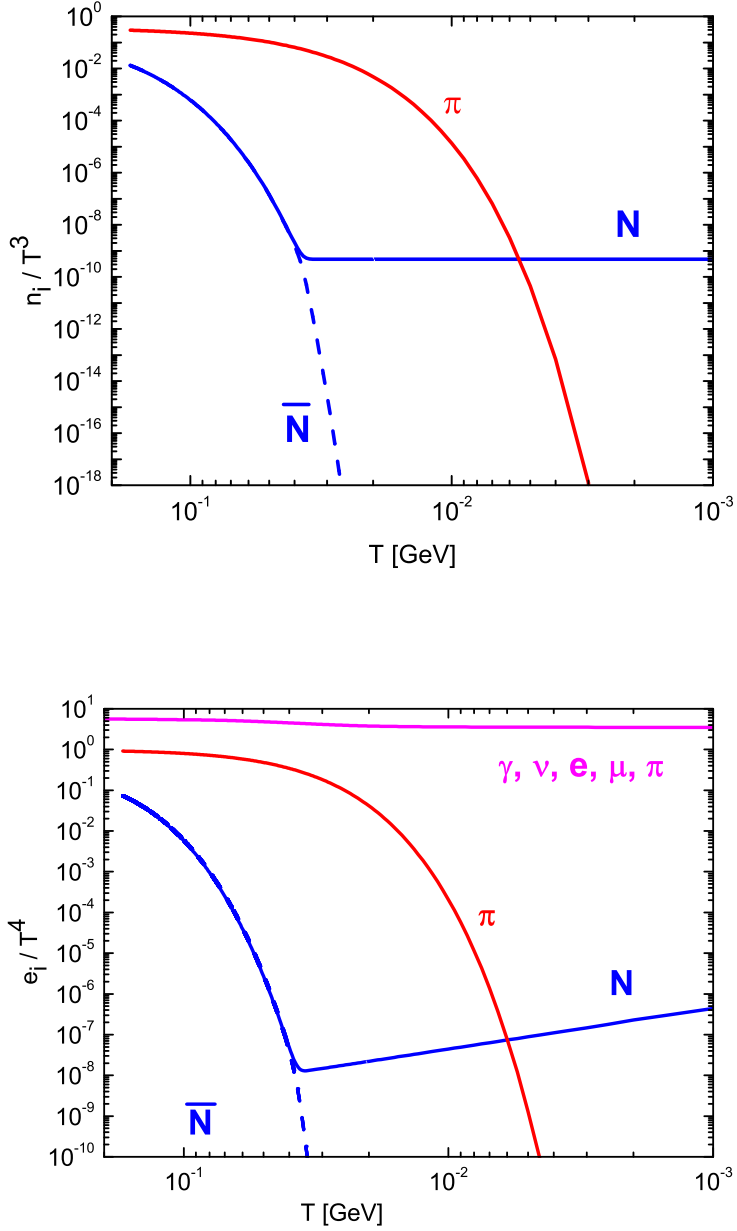


FIG. 7: (Color online) Evolution of scaled hadron densities $n_i/T^3 = Y_i s/T^3 \approx Y_i^{eq} s/T^3$ (top panel) and related energy densities (bottom panel; the top curve is for the electro-weak contribution (γ , ν 's, e , μ) + pions (π); the pion component is also depicted separately). Instead of p and \bar{p} , the densities of nucleons (N , n_+) and antinucleons (\bar{N} , n_-) are exhibited. For $\eta = 10^{-10}$.

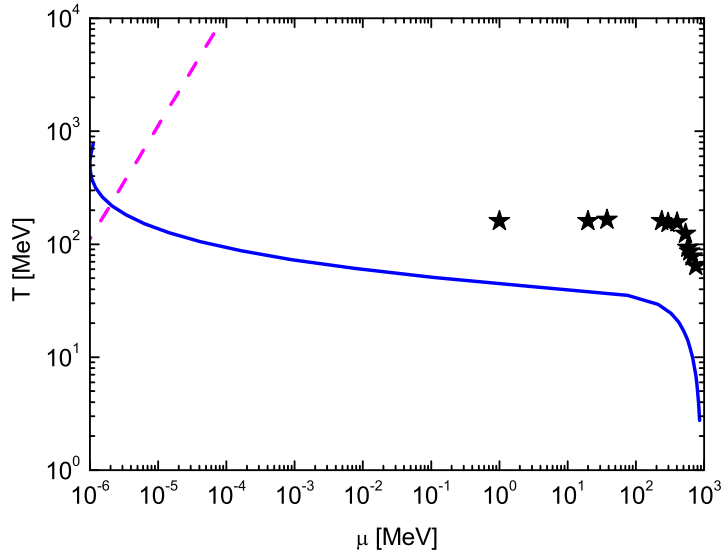


FIG. 8: (Color online) Adiabatic path of cosmic matter in the phase diagram of strongly interacting matter for $\eta = 10^{-10}$ (solid curve for confined matter, $h_{eff} = 10$). The straight upper section (dashed curve) is for an approximation of deconfined matter. (The crossing does not necessarily imply phase equilibrium. For the given approximations, the turn from deconfined to confined adiabatic paths is by a Maxwell like construction with mixed phase; these path sections are not displayed.) The asterisks depict chemical freeze-out points from [1] (first quotation, table 2-upper part, and LHC estimate mentioned in text there).